Published in final edited form as:

NMR Biomed. 2008 June ; 21(5): 473–478. doi:10.1002/nbm.1211.

Fractionated Manganese-Enhanced Magnetic Resonance Imaging

Nicholas A. Bock, **Fernando F. Paiva**, and **Afonso C. Silva**

Cerebral Microcirculation Unit/ Laboratory of Functional and Molecular Imaging/ National Institute of Neurological Disorders and Stroke/ National Institutes of Health, 10 Center Drive, Building 10, Room BD109, Bethesda, Maryland, United States, 20892-1065

Abstract

We investigated the use of manganese-enhanced magnetic resonance imaging (MEMRI) with fractionated doses as a way to retain the unique properties of manganese as a neuronal contrast agent while lessening its toxic effects in animals. First, we followed the signal enhancement on T_1-weighted images of the brains of rats receiving 30 mg/kg fractions of $MnCl_2{\cdot}4H_2O$ every 48 hours and found that the signal increased in regions with consecutive fractionated doses up to about six injections, then saturated. Second, we used T_1 mapping to test whether the amount of MRI-visible manganese that accumulated depended on the driving concentration of manganese in the fractions. For a fixed cumulative dose of 180 mg/kg $MnCl_2{\cdot}4H_2O$, increasing fraction doses of 6 × 30 mg/kg, 3 × 60 mg/kg, 2 × 90 mg/kg and 1 × 180 mg/kg produced progressively shorter T_1 values. The adverse health effects, however, also rose with the fraction dose. Thus, fractionated MEMRI can be used to balance the properties of manganese as a contrast agent in animals against its toxic effects.

Introduction

MRI excels in animal neuroimaging because of its intrinsic soft tissue contrast, high resolution, and ability to follow *in vivo* processes longitudinally; however, it lacks the breadth of reporters that are available to optical imaging techniques and positron emission tomography. Thus, there is great interest in MRI research to develop contrast agents that report on the cellular, molecular, and functional properties of tissue (1).

The metal manganese (atomic number 25) was one of the first contrast agents proposed for MRI (2) and is now widely used as a contrast agent for animal neuroimaging (3). The divalent ion (Mn^{2+}) has a similar ionic radius to calcium (Ca^{2+}) and mimics it in many biological systems. It is highly paramagnetic and is an excellent T_1-shortening agent. In the central nervous system, manganese is taken up by cells through voltage-gated calcium channels (4) where it accumulates with a half-life of 51–74 days in regions of the brain (5). Since its clearance rate is slow, its distribution can be investigated using lengthy, three dimensional, high resolution T_1-weighted pulse sequences. Manganese is especially useful at high fields, where the T_1 values in the brain become longer and less distinct between tissue types, reducing intrinsic contrast.

So far, three major applications of manganese-enhanced MRI (MEMRI) in animal neuroimaging have been described: *1* fiber tracking, *2* contrast enhancement in diverse brain regions, and *3* functional imaging. For applications besides fiber tracking, manganese is injected systemically either into the bloodstream (6), where it reaches the cerebral-spinal-fluid (CSF) via the choroid plexus, or directly into the CSF (7). The subsequent uptake in the brain leads to different manganese accumulations in regions (8) based on their neuronal density, function, and possibly the presence of divalent metal transporters (9). The resulting signal enhancement greatly improves contrast in T_1-weighted images and also the overall image signal-to-noise ratio (SNR), since manganese is taken up to some extent by all regions of the brain. This makes MEMRI ideal for high resolution studies of the whole brain where as many structures as possible must be delineated – for example, phenotyping genetically altered mice (10). It can also be used to generate contrast between healthy and pathological tissue (11–13).

As with any other contrast agent, the dose of manganese in the brain needs to be sufficiently high to generate contrast. Manganese, however, is toxic and produces both systemic and neurological effects at high doses. In humans and non-human primates, poisoning with the metal leads to a form of parkinsonism called manganism (14), likely caused by an accumulation in the structures of the basal ganglia (15). The neurological effects in rodents, however, are much less severe (16) and the danger is primarily from acute damage to the heart and the liver (17) – especially in models of disease like cancer or stroke where the animals' health is already compromised. A previous study in healthy mice has shown injections as high as 175 mg/kg (dry drug weight/body weight) of the hydrated salt, $MnCl_2{\cdot}4H_20$ produce excellent contrast in the brain (18). However, it is unlikely that sick or fragile transgenic animals will tolerate such a high dose. As well, high doses are not advisable for longitudinal studies requiring repeated imaging sessions.

The adverse effects of manganese can possibly be lessened by using a lower dose of manganese in combination with a pulse sequence that is sensitive to small changes in T_1 (19). It is more desirable, however, to improve manganese delivery to the brain for the best possible contrast while avoiding its systemic toxic effects. In the present work, we investigate the use of small fractionated injections of manganese as a way to build detectable doses in the brain while lessening the effects of acute exposure to other organs.

Materials and Methods

Experimental Design

It is known from toxicology studies that rats will tolerate daily injections of 30 mg/kg $MnCl_2{\cdot}4H_20$ for up to six weeks (20). We used this as our starting dose for fractionated experiments, but lengthened the period between injections to 48 hours to allow the manganese to clear from the heart (21) and further limit toxicity.

Two separate experiments were carried out. First, in a group of four rats, we followed the contrast enhancement in 3D T_1-weighted images of the whole brain for a series of 12 × 30 mg/kg injections to a total cumulative dose of 360 mg/kg. Then, to study the effects of the dose of the fractions on detectable manganese accumulation, we performed whole-brain

quantitative T_1-mapping in four groups of four rats at a cumulative dose of 180 mg/kg, delivered either in a single dose or in fractions of 6 × 30, 3 × 60, or 2 × 90 mg/kg. We also acquired T_1-weighted images in these rats for qualitative analysis.

Animal Preparation

All animal experiments were approved by the NINDS/NIDCD Animal Care and Use Committee. Experiments were carried out in 21 adult male Sprague-Dawley rats weighing 250–350 grams. A solution of $MnCl_2$ (Sigma Aldrich, St. Louis, MO, USA) was prepared at a concentration of 100 mM Mn^{2+} in distilled water and buffered to pH 7.4 using bicine (Sigma Aldrich, St. Louis, MO, USA) (22), since Mn^{2+} in solution is a weak acid. To reduce stress to the heart, higher dose fractions of 90 and 180 mg/kg were injected intravenously in the tail vein at a rate of 1.25 ml/hour (18) with the rats anaesthetized on 2% isoflurane. For low dose fractions of 30 and 60 mg/kg, the solution was diluted in saline to 25 mM Mn^{2+} and injected intraperitoneally. Animals were returned to their cages after dosing with free access to food and water.

During imaging, the rats were placed on an MRI-compatible cradle and anesthetized through a nose cone with 2% isofluorane in a 2:2:1 mixture of medical air, nitrogen, and oxygen. The rectal temperature was monitored and the animal was heated to 37°C using a resistive heating pad. All imaging was performed 48 hours after the last manganese injection.

T_1-Weighted MRI

Whole-brain T_1-weighted MRI was performed on a 7T MRI scanner (Bruker Biospin, Ettlingen, Germany) equipped with an 15 cm gradient set of 450 mT/m strength (Resonance Research Inc., Billerica, MA). A custom-built 16-rung high pass birdcage coil with a 12 cm inner diameter was used for transmission, and a four-element phased-array receive coil (Bruker Biospin, Ettlingen, Germany) for reception. The T_1-weighted sequence was a 3D fast spin-echo with two echoes, and an isotropic resolution of 167 μm (TE = 12 ms, TR = 150 ms, FOV = 42.8 × 32.0 × 32.0 mm, Matrix = 256 × 128 × 128, Number of averages = 2). B_1 inhomogeneities were corrected using the following reference coil method (23). The B_1 field of the large birdcage coil was considered homogenous over the rat brain. A low resolution image (64 × 32 × 32) was made using the birdcage coil for reception with the same parameters as the high resolution image using the phased-array coil. The corrected image, $I_{corrected}$, was given by:

$$I_{corrected} = \frac{I_{phased}}{\left(\frac{I_{phased,smoothed}}{I_{birdcage,smoothed}}\right)} \quad (1)$$

where I_{phased} was the image from the phased array coil, and $I_{phased,smoothed}$ and $I_{birdcage,\ smoothed}$ were B-spline smoothed images from the phased array and birdcage coils respectively.

T_1 Mapping

Whole-brain T_1 mapping was performed using a quadrature surface coil (RAPID Biomedical GmbH, Rimpar, Germany) and a 2D inversion-recovery EPI sequence with an

in-plane resolution of 267 μm and a slice thickness of 750 μm (TE = 38 ms, TR = 9400 ms, FOV = 25.6 × 25.6 mm, Matrix = 96 × 96, Number of slices = 5, Number of inversion times = 30, Inversion time increment = 300 ms, Number of averages = 4). The data was fit to a three parameter, single-exponential T_1 recovery function in Matlab (MathWorks, Natick, MI, USA).

Data Analysis and Statistics

All 3D images were registered into a common space using an affine registration and analyzed in Amira (Mercury Computer Systems, Houston, TX, USA). Region-of-interest (ROI) analysis was performed on the T_1-weighted images and the 2D T_1 maps in Amira. ROIs as shown in Figure 1 were drawn in structures identified by an atlas (24) that could be clearly delineated in both the T_1-weighted images and the lower-resolution T_1 maps, from which mean signal intensities and T_1s were measured, respectively. For each ROI in each rat, the mean signal intensity from the T_1-weighted image was normalized to the mean signal intensity in muscle surrounding the skull. Significant differences across the different doses were computed using a non-parametric analysis of variance (Kruskal-Wallis), performed in Excel (Microsoft, Redmond, WA, USA) using Analyze-It (Analyse-It Software Ltd., Leeds, England), followed by a Bonferonni multiple-comparison test. Significance levels were set at $p < 0.05$.

Results

Figure 2 shows representative slices from the images of the rats receiving 30 mg/kg fractionated injections of $MnCl_2{\cdot}4H_20$. Compared to the control images, a robust signal enhancement of major areas of the brain, such as the olfactory bulbs, hippocampus, hypothalamus, thalamus, striatum, inferior colliculus and cortex is observed with the first fraction of 30 mg/kg (data not shown). A progressive signal enhancement occurs up to a cumulative dose of 6 × 30 mg/kg, above which there is no visible improvement in overall brain enhancement. The dose course of T_1-weighted signal enhancement shows that, in all tested regions, the signal enhancement in the brain increases with the number of injected fractions and the MRI signal is significantly higher than in the control animals at doses of 3 × 30 mg/kg and above ($p \leq 0.05$). There were no significant differences in signal enhancement at doses of 6 × 30 mg/kg and higher, indicating saturation of the accumulation of manganese in all regions.

To test if the dose of the individual manganese fractions affected the total manganese accumulation, we injected four groups of four rats each to a cumulative injected dose of 180 mg/kg using fractionated doses of 3 × 60, 2 × 90, and 1 × 180 mg/kg $MnCl_2{\cdot}4H_20$. Figure 3 shows coronal and horizontal slices from a whole-brain T_1-weighted image of a control rat and a representative rat for each fractionation schedule. Not only does the image enhancement increase with the dose of the fractions, but the contrast between fine structures becomes better. This can be readily seen as improved definition between layers of the cortex. This indicates that an increase in the driving gradient of manganese between the blood and the brain tissue leads to an increase in manganese uptake for a fixed cumulative dose. Figure 3 also shows the T_1 values we measured in regions of the brain for each

fractionation schedule. In all regions of all groups injected with manganese, the T_1 is significantly smaller than in the corresponding region of the control group ($p < 0.05$), indicating an effective accumulation of manganese in the brain. There is a clear trend towards shorter T_1s with increasing fraction doses. However, no statistically significant differences are seen between the different injected groups We were not able to test whether the relaxation rate ($1/T_1$) in regions of the brain saturated with the dose of the fractions, because individual doses higher than 180 mg/kg would have been toxic to the animals.

To investigate the mitigating effects of fractionation on the toxicity of manganese, we monitored and scored the rats daily over the course of injections for changes in weight, attitude and activity, appetite and hydration, gait and posture, appearance, and complications at the injection site. For some fractionation schedules, we injected more animals than we imaged. Table 1 summarizes our findings across the groups. In all groups, the rats lost weight after the first injections but not below 10% of their initial weight. In the 30 mg/kg rats injected to 6 doses, the rats began regaining weight and ended the study heavier overall (mean net weight gain of 10% ± 2% ($\mu \pm \sigma$), n = 6). None of the other groups showed weight gain, although there might not have been enough time in the injection course for the early weight loss to reverse. The manganese at doses of 60 mg/kg and above produced toxic effects at the injection site. In the intraperitoneally-injected rats, some animals (n = 2/6) developed an induration that eventually led to substantial bleeding inside the abdominal wall. This seemed to occur because the intraperitoneal injection was not deep enough, allowing some manganese to deposit subcutaneously. In the intravenously-injected animals that received 90 mg/kg fractions, severe necrosis sometimes was seen below the injection site on the tail (n = 2/6). This symptom was present in every rat injected with the single 180 mg/kg fraction. Although the manganese solution was isotonic and buffered to a physiological pH, it appeared that the metal itself had a toxic effect on contact with tissue; therefore, the safest route of application was a low concentration solution of $MnCl_2$ injected into the large volume of the intraperitoneal cavity. As well, one of the five rats being injected with a single 180 mg/kg fraction died of apparent heart failure and all were hunched and lethargic 48 hours following the injection and were sacrificed immediately after imaging at the recommendation of a veterinarian.

Discussion and Conclusions

We found that the MRI-visible concentration of Mn^{2+} in the brain increases as the number of consecutive fractionated doses increases, although the signal enhancement obtained on T_1-weighted images eventually saturates. Moreover, the T_1-shortening at a fixed cumulative dose increases with the dose of the individual fractions. Taken together, both findings indicate that the amount of manganese that ultimately accumulates in the parenchyma depends on the concentration gradient of manganese between blood and brain tissue. Higher fractional doses deliver more manganese to tissue at each application. On the other hand, the accumulation of manganese in the parenchyma with each dose reduces the driving gradient, causing the eventual saturation of signal enhancement shown in Fig. 2. The systemic toxic effects of the manganese, however, become worse at higher fraction doses. Therefore, the best approach for researchers planning a fractionated MEMRI study in novel animal models is to empirically find the highest fraction dose the animals will tolerate health-wise, and then

determine the number of fractionated injections needed to fully enhance the signal. We found that for 30 mg/kg fractions, the animals' health appeared normal, even after twelve injections, and the dose produced satisfactory image enhancement; thus, it should be possible to obtain image enhancement with manganese even in fragile animals or those with compromised health.

As well as enhancing contrast for single anatomical images of animals, fractionated MEMRI could be used for other applications. For longitudinal studies, it could be useful for maintaining image enhancement in multiple imaging sessions over the duration of a study – especially if the manganese helped to identify the margins of disease. Fractionated MEMRI could also be used in tract tracing studies. A current problem with manganese as a tract tracer is that it does not always reveal the entire neuronal pathway. For instance, manganese injected in the vitreous of the eye in the rat does not reach the primary visual cortex and is only detected as far as the superior colliculus (8). Axonal transport distance can be increased by electrically stimulating nuclei in a pathway (25), but it is also possible that repeated fractions of manganese could be used to maintain a supply of manganese for transport along an entire tract. Finally, fractionated MEMRI may also be useful for functional studies. The ability of manganese to act as surrogate marker for calcium influx provides functional information in the brain (4, 26). The manganese injection and functional stimulation can be administered outside the magnet and the uptake imaged later, which avoids the complications of performing functional stimulations inside the magnet (27). Fractionated MEMRI could be useful here for two reasons. First, the multiple injection periods allow for multiple stimulations to be performed in animals, increasing the total time each animal is stimulated with manganese in its system. Second, if imaging is performed throughout the dose course, the information in the signal enhancement or T_1 curves may be used to identify regions of activity. For instance, the slope of the signal enhancement curve may be steeper in active areas of the brain. One interesting inference stemming from the saturation of the signal enhancement with cumulative doses of manganese is that, in applications where a constant slope is desired, progressively higher doses need to be administered in order to maintain the driving gradient constant. It should be possible to model the uptake curve of manganese in order to predict the dosage scheme necessary to achieve a constant rate of signal enhancement, a subject of future studies.

Overall, fractionated MEMRI will allow the unique properties of manganese as a contrast agent to be used in a wider variety of neuroscience models.

Acknowledgments

The authors would like to acknowledge the excellent technical assistance of Mrs. Julie Mackel. This research was supported by the Intramural Research Program of the NIH, NINDS (Alan P. Koretsky, Scientific Director).

References

1. Jasanoff A. Functional MRI using molecular imaging agents. Trends Neurosci. 2005; 28(3):120–126. [PubMed: 15749164]
2. Lauterbur PC. Image Formation by Induced Local Interactions - Examples Employing Nuclear Magnetic-Resonance. Nature. 1973; 242(5394):190–191.

3. Koretsky AP, Silva AC. Manganese-enhanced magnetic resonance imaging (MEMRI). NMR Biomed. 2004; 17(8):527–531. [PubMed: 15617051]

4. Lin YJ, Koretsky AP. Manganese ion enhances T1-weighted MRI during brain activation: an approach to direct imaging of brain function. Magn Reson Med. 1997; 38(3):378–388. [PubMed: 9339438]

5. Takeda A, Sawashita J, Okada S. Biological half-lives of zinc and manganese in rat brain. Brain Res. 1995; 695(1):53–58. [PubMed: 8574647]

6. Silva AC, Lee JH, Aoki I, Koretsky AP. Manganese-enhanced magnetic resonance imaging (MEMRI): methodological and practical considerations. NMR Biomed. 2004; 17(8):532–543. [PubMed: 15617052]

7. Liu CH, D'Arceuil HE, de Crespigny AJ. Direct CSF injection of MnCl(2) for dynamic manganese-enhanced MRI. Magn Reson Med. 2004; 51(5):978–987. [PubMed: 15122680]

8. Natt O, Watanabe T, Boretius S, Radulovic J, Frahm J, Michaelis T. High-resolution 3D MRI of mouse brain reveals small cerebral structures in vivo. J Neurosci Methods. 2002; 120(2):203–209. [PubMed: 12385770]

9. Thompson K, Molina RM, Donaghey T, Schwob JE, Brain JD, Wessling-Resnick M. Olfactory uptake of manganese requires DMT1 and is enhanced by anemia. FASEB J. 2007; 21(1):223–230. [PubMed: 17116743]

10. Bock NA, Kovacevic N, Lipina TV, Roder JC, Ackerman SL, Henkelman RM. In vivo magnetic resonance imaging and semiautomated image analysis extend the brain phenotype for cdf/cdf mice. J Neurosci. 2006; 26(17):4455–4459. [PubMed: 16641223]

11. Wei Q, Clarke L, Scheidenhelm DK, Qian B, Tong A, Sabha N, Karim Z, Bock NA, Reti R, Swoboda R, Purev E, Lavoie JF, Bajenaru ML, Shannon P, Herlyn D, Kaplan D, Henkelman RM, Gutmann DH, Guha A. High-grade glioma formation results from postnatal pten loss or mutant epidermal growth factor receptor expression in a transgenic mouse glioma model. Cancer Res. 2006; 66(15):7429–7437. [PubMed: 16885338]

12. Henning EC, Meng X, Fisher M, Sotak CH. Visualization of cortical spreading depression using manganese-enhanced magnetic resonance imaging. Magn Reson Med. 2005; 53(4):851–857. [PubMed: 15799040]

13. Aoki I, Naruse S, Tanaka C. Manganese-enhanced magnetic resonance imaging (MEMRI) of brain activity and applications to early detection of brain ischemia. NMR Biomed. 2004; 17(8):569–580. [PubMed: 15617055]

14. Pal PK, Samii A, Calne DB. Manganese neurotoxicity: a review of clinical features, imaging and pathology. Neurotoxicology. 1999; 20(2–3):227–238. [PubMed: 10385886]

15. Dobson AW, Erikson KM, Aschner M. Manganese neurotoxicity. Ann N Y Acad Sci. 2004; 1012:115–128. [PubMed: 15105259]

16. Dodd CA, Ward DL, Klein BG. Basal Ganglia accumulation and motor assessment following manganese chloride exposure in the C57BL/6 mouse. Int J Toxicol. 2005; 24(6):389–397. [PubMed: 16393931]

17. Gerber GB, Leonard A, Hantson P. Carcinogenicity, mutagenicity and teratogenicity of manganese compounds. Crit Rev Oncol Hematol. 2002; 42(1):25–34. [PubMed: 11923066]

18. Lee JH, Silva AC, Merkle H, Koretsky AP. Manganese-enhanced magnetic resonance imaging of mouse brain after systemic administration of MnCl2: dose-dependent and temporal evolution of T1 contrast. Magn Reson Med. 2005; 53(3):640–648. [PubMed: 15723400]

19. Chuang KH, Koretsky A. Improved neuronal tract tracing using manganese enhanced magnetic resonance imaging with fast T(1) mapping. Magn Reson Med. 2006; 55(3):604–611. [PubMed: 16470592]

20. Zhang S, Zhou Z, Fu J. Effect of manganese chloride exposure on liver and brain mitochondria function in rats. Environ Res. 2003; 93(2):149–157. [PubMed: 12963399]

21. Takeda A, Sawashita J, Okada S. Manganese concentration in rat brain: manganese transport from the peripheral tissues. Neurosci Lett. 1998; 242(1):45–48. [PubMed: 9510001]

22. Morita H, Ogino T, Fujiki N, Tanaka K, Gotoh TM, Seo Y, Takamata A, Nakamura S, Murakami M. Sequence of forebrain activation induced by intraventricular injection of hypertonic NaCl

detected by Mn2+ contrasted T1-weighted MRI. Auton Neurosci. 2004; 113(1–2):43–54. [PubMed: 15296794]

23. Wang J, Qiu M, Constable RT. In vivo method for correcting transmit/receive nonuniformities with phased array coils. Magn Reson Med. 2005; 53(3):666–674. [PubMed: 15723397]
24. Paxinos, G.; Watson, C. The Rat Brain in Stereotaxic Coordinates. New York: Academic Press; 1998.
25. Bilgen M, Peng W, Al-Hafez B, Dancause N, He YY, Cheney PD. Electrical stimulation of cortex improves corticospinal tract tracing in rat spinal cord using manganese-enhanced MRI. J Neurosci Methods. 2006; 156(1–2):17–22. [PubMed: 16530270]
26. Kuo YT, Herlihy AH, So PW, Bell JD. Manganese-enhanced magnetic resonance imaging (MEMRI) without compromise of the blood-brain barrier detects hypothalamic neuronal activity in vivo. NMR Biomed. 2006; 19(8):1028–1034. [PubMed: 16845705]
27. Yu X, Wadghiri YZ, Sanes DH, Turnbull DH. In vivo auditory brain mapping in mice with Mn-enhanced MRI. Nat Neurosci. 2005; 8(7):961–968. [PubMed: 15924136]

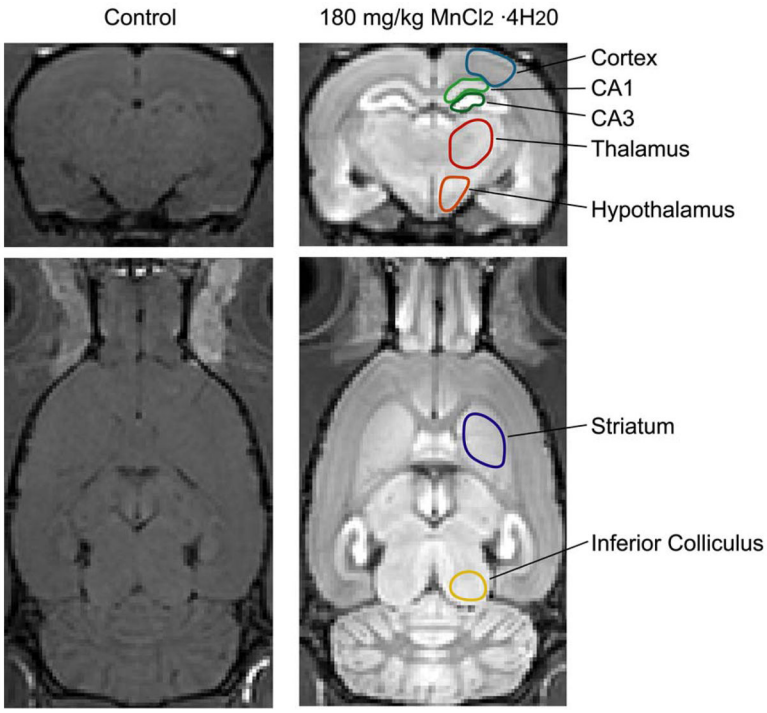

Figure 1.

Region-of-interest (ROI) definitions for different brain structures. Representative coronal **(Top)** and horizontal **(Bottom)** slices from a 3D T_1-weighted image of a control rat and a rat following a 180 mg/kg injection of $MnCl_2 \cdot 4H_20$ showing regions analyzed in the study. Each region extends through multiple slices and corresponding ROIs were also defined in the coronal T_1 maps.

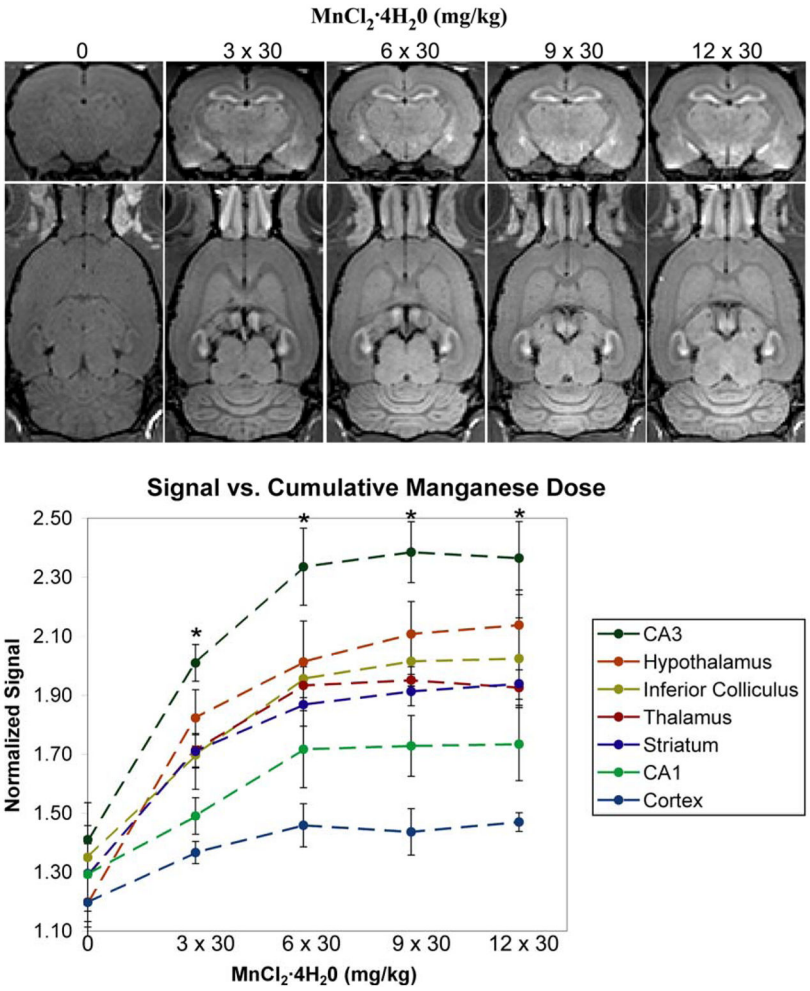

Figure 2.

The effect of increasing numbers of fractions of $MnCl_2 \cdot 4H_20$ on the magnitude signal intensity in T_1-weighted images. **(Top)** Representative coronal and horizontal slices from 3D T_1-weighted images of a rat at each cumulative dose. **(Bottom)** A graph showing the magnitude signal from each brain region normalized to its value in the muscle surrounding the skull (error bars are standard deviations, n=4). The asterix denotes the manganese-injected groups of rats were significantly different from the control group ($p \leq 0.05$) – there were no significant differences between the injected groups.

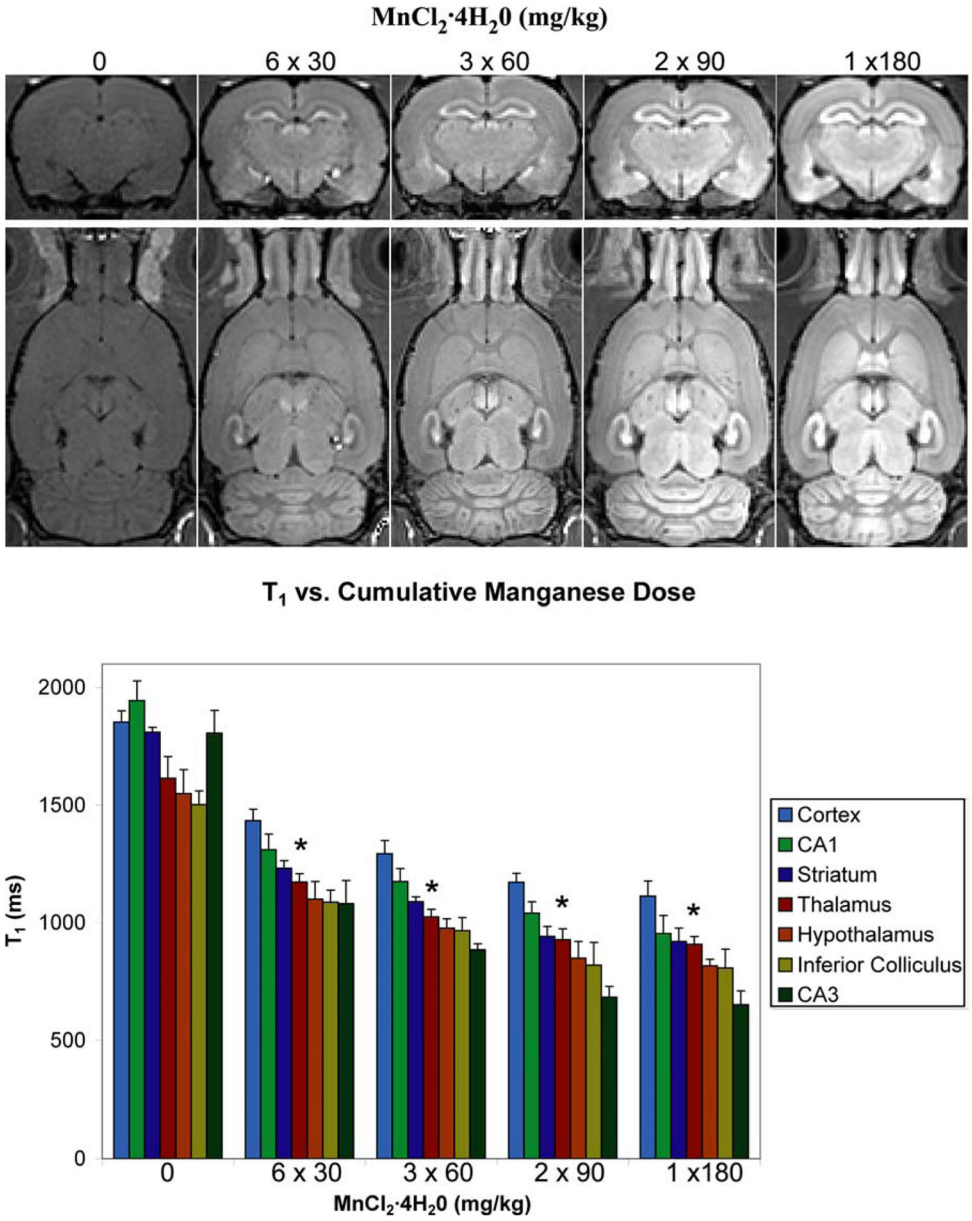

Figure 3.

The effect of increasing the dose of fractions of $MnCl_2 \cdot 4H_20$ on T_1 and magnitude signal intensity in T_1-weighted images. **(Top)** Representative coronal and horizontal slices from 3D T_1-weighted images of rat at each dose fraction. **(Bottom)** The T_1 in regions of the brain for control rats and rats from each dose fraction group at a total cumulative dose of 180 mg/kg $MnCl_2 \cdot 4H_2O$ (error bars are standard deviations, n = 4). The asterix denotes the manganese-injected groups of rats were significantly different from the control group ($p \leq 0.05$) – there were no significant differences between the injected groups.

Table 1

Health assessment of rats for each of the different fraction dose cases. (iv denotes an intravenous injection in the tail, ip denotes an intraperitoneally injection.)

Fraction Course (mg/kg $MnCl_2 \cdot 4H_20$)	6 × 30	3 × 60	2 × 90	1 × 180
Observation Period (days)	12	6	4	2
Number of Rats Injected	6	6	4	5
Injection Route	iv	iv	ip	ip
Weight	Early loss. Later gain.	Early loss.	Early loss.	Early loss.
Deaths	0	0	0	1
Injection site complications.	None.	Occasional abdominal induration.	Occasional tail necrosis.	Consistent tail necrosis.
Appearance.	Normal.	Normal.	Normal.	Rumpled and hunched.
Activity	Normal.	Normal.	Normal.	Lethargic.